Smart Structures and Systems, *Vol. 15, No. 6 (2015) 1625-1642*
DOI: http://dx.doi.org/10.12989/sss.2015.15.6.1625

Self-reliant wireless health monitoring based on tuned-mass-damper mechanism

Kanjuro Makihara[*1a], Hidekazu Hirai[2], Yuta Yamamoto[1] and Hisao Fukunaga[1]

[1]*Tohoku University, Department of Aerospace Engineering, 6-6-01 Aramaki-Aza-Aoba, Aoba-Ward, Sendai, 980-8579 Japan*
[2]*Shinko Electric Industries Co., Ltd., 80, Oshimada-Machi, Nagano, 381-2287 Japan*

(Received July 21, 2013, Revised January 24, 2014, Accepted February 15, 2014)

Abstract. We propose an electrically self-reliant structural health monitoring (SHM) system that is able to wirelessly transmit sensing data using electrical power generated by vibration without the need for additional external power sources. The provision of reliable electricity to wireless SHM systems is a highly important issue that has often been ignored, and to expand the applicability of various wireless SHM innovations, it will be necessary to develop comprehensive wireless SHM devices including stable electricity sources. In light of this need, we propose a new, highly efficient vibration-powered generator based on a tuned-mass-damper (TMD) mechanism that is quite suitable for vibration-based SHM. The charging time of the TMD generator is shorter than that of conventional generators based on the impedance matching method, and the proposed TMD generator can harvest 16 times the amount of energy that a conventional generator can. The charging time of an SHM wireless transmitter is quantitatively formulated. We conduct wireless monitoring experiments to validate a wireless SHM system composed of a self-reliant SHM and a vibration-powered TMD generator.

Keywords: wireless health monitoring; self-reliant energy harvester; vibration-powered generator; tuned-mass-damper mechanism

1. Introduction

1.1 Research background

As vibration is a major source of building degradation and structural soundness loss, structural health monitoring (SHM) is an important practice in keeping vibrating structures healthy (Carden and Fanning 2004, Hu *et al*. 2012, Chong *et al*. 2010, Fan and Qiao 2011). Wireless health monitoring is a very promising form of SHM system that can reduce the complexity of wire networks (Li *et al*. 2010, Cho *et al*. 2010, Lynch 2005). However, providing reliable electricity to the monitoring systems is a practical, vitally significant problem that has often not been carefully considered in the actual application of wireless SHM to real structures. Because it is difficult to attach long wires to isolated structures, moving vehicles, long bridges, elevated expressways, or rotating devices such as turbine blades or automobile tires, the use of vibration-powered

∗Corresponding author, Associate Professor, E-mail: makihara@ssl.mech.tohoku.ac.jp

http://www.techno-press.org/?journal=sss&subpage=8 ISSN: 1738-1584 (Print), 1738-1991 (Online)

generation (energy harvesting on the basis of vibration)is a reasonable means of powering monitoring devices. Vibration-powered generators can also be used structurally as electrically self-reliant energy harvesters to power wireless monitoring and, as such, independent energy harvesters are particularly suitable for use in structural health monitoring applications for which wireless monitoring is desirable.

To date, vibration-powered generation research has focused mainly on increasing the efficiency of vibration-powered generators that use piezoelectric transducers. As a departure from the simplest harvester design, a conventional DC power generator uses only a diode bridge, often called a standard rectifier (Beeby and White 2010, Kazmierski and Beeby 2010), to effect simple AC-to-DC power conversion. Kong *et al*. (2010) presented a resistive impedance matching circuit for piezoelectric energy harvesting. Ottman *et al*. (2003) added an adaptive circuit and a switching DC/DC step-down converter preceded by a capacitive filter to this conventional energy harvester, while Lesieutre *et al*. (2003) described in detail the effects of damping in harvesting electrical power from a mechanically excited piezoelectric structure. Kim *et al*. (2005) outlined the structural factors that maximize electrical power output under a given set of constraints. An approach using a tuned auxiliary structure presented by Cornwell *et al*. (2005) and Lefeuvre *et al*. (2007) improved output power by changing the load resistance, which depends on the base acceleration amplitude and frequency. Wu *et al*. (2009) studied the transient behavior of several energy-harvesting circuits using lead zirconate titanate (PZT) transducers and a storage capacitor. In order to surpass the power output of standard energy harvesting circuits, Guyomar *et al*. (2005) proposed synchronized switch harvesting on an inductor (SSHI), which adds a nonlinear circuit element to the conventional harvesting circuit. Badel *et al*. (2006) achieved a four-fold increase in generated power by replacing the standard circuit with an SSHI circuit. The output power of four different conditioning SSHI circuits was compared by Qiu *et al*. (2009). Finally, Shen *et al*. (2010) presented a technique for optimized energy harvesting called enhanced synchronized switch harvesting (ESSH), a process that involves nonlinear harvesting from structural vibration.

Past research on increasing the power generation efficiency of vibration-powered generation has centered upon two types of methods: impedance matching methods using optimized resistors (Kong *et al*. 2010, Ottman *et al*. 2003, Lesieutre *et al*. 2003, Kim *et al*. 2005, Cornwell *et al*. 2005, Lefeuvre*et al*. 2007, Wu *et al*. 2009) and switching circuit methods utilizing electric switches (Guyomar *et al*. 2005, Badel *et al*. 2006, Makihara *et al*. 2006, Qiu *et al*. 2009, Shen *et al*. 2010). While impedance matching has the critical disadvantage of working well only at an optimal value of resistance, switching circuit methods also face disadvantages in that they require external power sources to both perform the switching action and activate the PCs, filters, and sensors used for switch control. Although the large amount of power needed to activate arrays of peripheral electric devices is often not accounted for, it should not be ignored in real applications.

1.2 Research objectives

In performing wireless SHM, the provision of reliable electricity to the wireless SHM system is a highly important requirement that is often ignored in practice. In order to expand the application range of various wireless SHM innovations, it will be necessary to develop and discuss comprehensive wireless SHM devices including stable electricity sources.

To solve such problems, we propose an electrically self-reliant harvester that is suitable for vibration-based SHM systems. The main objective of this paper is to describe an electrically self-reliant SHM system that can power the wireless transmission of sensing data using only the electrical energy produced by a vibration-powered generator. Fig. 1 shows the concept underlying the proposed scheme. The system is composed of a vibrating structure consisting of a PZT and a sensor, a vibration-powered generator, and a radio transmitter. In order to successfully develop this self-reliant system, however, the power generation performance of the vibration-powered generator must be improved.

To achieve this, three research objectives have been set. First, a new, highly efficient vibration-powered generator must be developed. This effort will include conducting a detailed comparison of the differences between serial and parallel connections in formulating the electrical circuit. Next, a wireless monitoring system consisting of a sensor, a peripheral interface controller (PIC), and a wireless transmitter will be fabricated. Finally, the feasibility of using the electrically self-reliant SHM systems to perform wireless monitoring must be assessed.

2. Development of vibration-powered generation

2.1 Piezoelectric transducer for vibration-powered generator

To achieve the goals of this study, it is of interest to develop a power generator that can utilize a piezoelectric transducer to convert vibrational energy into electrical energy. Such a transducer would be attached to the host structure and deform in accordance with structural vibration. Fig. 2 shows a simple vibration-powered generator with a piezoelectric transducer and a diode bridge. The piezoelectric transducer is modeled as a series-connected voltage source and a capacitor with a piezoelectric coefficient of b_t and a piezoelectric capacitance at a constant charge of C_t. Other parameters are the elongation of the piezoelectric transducer, x; the voltage generated by the piezoelectric transducer, V_t; the electric load, R; and the voltage at electric load, V_R. The piezoelectric transducer converts vibrations into an alternating current that is rectified to a direct current by the diode bridge, with the resulting electrical power consumed by the electric load. The basic equations of a piezoelectric transducer (Makihara *et al*. 2012) are

$$f_t = K_t x - b_t Q, \tag{1}$$

$$V_t = -b_t x + \frac{Q}{C_t}, \tag{2}$$

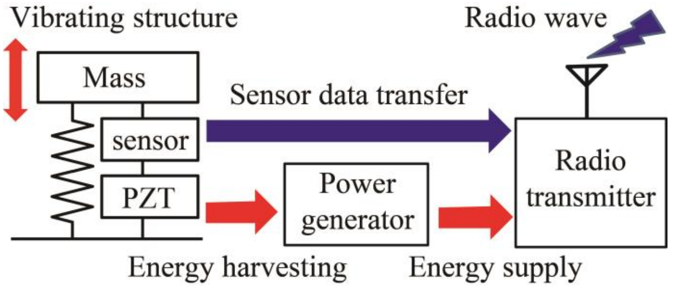

Fig. 1 Self-reliant monitoring system for wireless SHM with vibration-powered generator

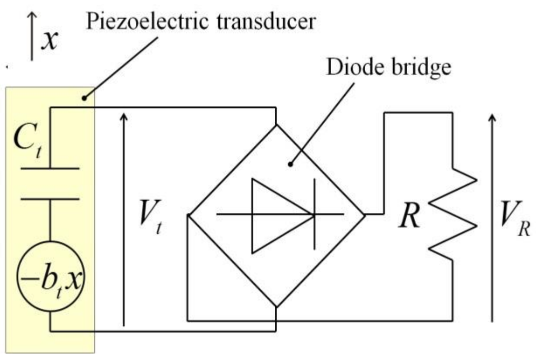

Fig. 2 Model of vibration-powered generator using piezoelectric transducer

where f_t is the force generated in the piezoelectric transducer, Q is the electric charge, and K_t is the stiffness at constant charge.

2.2 Vibration-powered generator based on impedance matching method

To maximize the power harvested at load resistor R in the circuit shown in Fig. 2, the load resistance value must match the impedance in the piezoelectric transducer. This is called impedance matching (IM) (Kong *et al*. 2010) and is optimized at a resistance given by

$$R = \frac{1}{\omega_t C_t}, \tag{3}$$

where ω_t is the angular frequency of the vibration applied to the piezoelectric transducer. At impedance matching, a maximum power level of

$$W_R = \frac{1}{R}\left(\frac{V_R}{\sqrt{2}}\right)^2 \tag{4}$$

can be harvested. The harvested power of the IM generator can be increased by increasing the voltage V_R at the resistor.

2.3 Vibration-powered generator used in TMD mechanism

Several studies have proposed an electrical tuned mass damper (TMD) with a piezoelectric transducer (Hagood and Flotow 1991, Wu 1996) inspired by the mechanical TMD mechanism. Both the electrical and the mechanical variants of the TMD mechanism can skillfully use the resonance of two vibrating systems, and a number of successive studies have proposed systems in which active elements based on the TMD mechanism, e.g., active-passive hybrid piezoelectric networks (Morgan and Wang 2002, Makihara *et al*. 2007, Wang and Inman 2011), are combined. Hybrid networks can be implemented using continuously variable elements such as voltage sources, charge sources, and variable resistors. They can provide satisfactory suppression performance, although they also require very expensive and complicated equipment.

Quite recently, Kozlowski *et al*. (2011) used sophisticated control theory to derive the stability requirements for a vibration control system based on a TMD circuit. The TMD mechanism is indeed more complex than it might appear, and much study remains in order to better understand it. Fig. 3 shows an electrical TMD model with a host structure; here, M_s, K_s, D_s, and x_s represent the mass, spring constant, damping coefficient, and elongation of the structure, respectively. The induced voltage V_x ($=-b_t x_s$) is proportional to the piezoelectric elongation, while f_s is the force applied to the host structure. Based on Eqs. (1) and (2), the equations of motion for an electrical TMD with a resistor and an inductor connected in series are given by

$$M_s\ddot{x}_s + D_s\dot{x}_s + \left(K_s + K_t\right)x_s - b_t Q = f_s, \tag{5}$$

$$L\ddot{Q} + R\dot{Q} + \frac{Q}{C_t} = b_t x_s. \tag{6}$$

An inductance-capacitance resistance (LCR) circuit has resonance properties similar to those of a mechanical TMD. For the purpose of TMD tuning, the fixed point theory (Hartog 1984) is often used to produce a resonance effect over a range of frequencies. This study focuses only on the first vibrational mode of the host structure, and therefore, for the purposes of power generation, the vibrational frequency of the TMD is set at the first mode. The single-inductor circuits in Figs. 5 and 6, which are based on the methodology proposed by Hagood and von Flotow (1991), cannot handle multiple-mode vibrations. As, according to Hollkamp (1994), a more complex electric circuit would be needed to generate power from multiple-mode vibrations, this is outside the scope of this study.

There are two approaches in considering which type of vibration-powered generator to use for an electrical TMD. The first involves using a serial connection between the inductor L and an electrical load R (Fig. 3), while the second involves connecting L and R in parallel. Three types of power-generation circuits (stand-alone piezoelectric transducer, serial TMD connection, and parallel TMD connection) are shown in Figs. 4-6, respectively. When the host structure vibrates at a frequency of ω_x, an induced voltage of

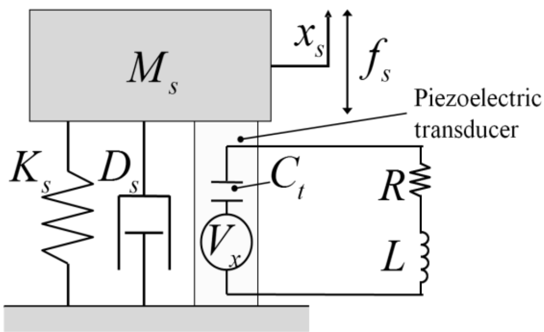

Fig. 3 Model of TDM using piezoelectric transducer

$$V_x \equiv V_{xm} \sin \omega_x t \tag{7}$$

is generated, where V_{xm} is the maximum voltage value. By applying Thevenin's theorem to the circuits on the left-hand sides of Figs. 4-6, each can be simplified into the equivalent circuits on the right-hand sides consisting of power supplies with alternating current sources and internal impedance elements. The voltage source V_p, impedance Z_p, and current I_p of an equivalent power supply are shown in Fig. 4 and are described using

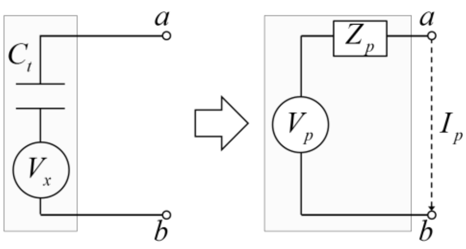

Fig. 4 Equivalent circuit of standalone piezoelectric generator

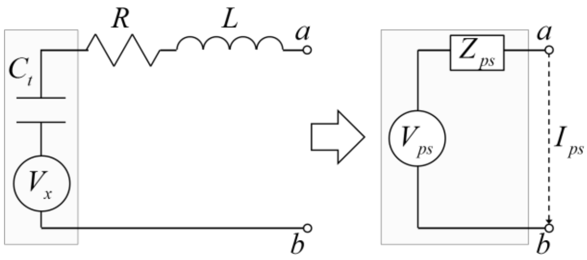

Fig. 5 Equivalent circuit of serial TMD generator

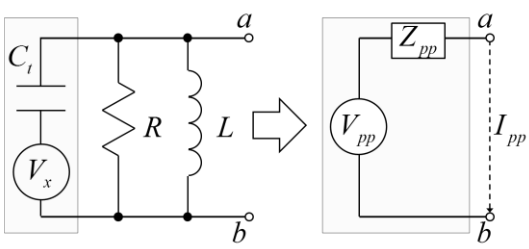

Fig. 6 Equivalent circuit of parallel TMD generator

$$V_{\mathrm{p}} = V_x, \tag{8}$$

$$Z_{\mathrm{p}} = \frac{1}{\omega_x C_{\mathrm{t}}}, \tag{9}$$

$$\left| I_{\mathrm{p}} \right| \equiv \left| \frac{V_{\mathrm{p}}}{Z_{\mathrm{p}}} \right| = V_{x\mathrm{m}} \omega_x C_{\mathrm{t}}, \tag{10}$$

where I_{p} is the current flow when terminals *a* and *b* are connected.

2.4 Serial TMD generator

For the serial TMD connection shown in Fig. 5, the electrical damping ratio of the LCR serial circuit, ζ_{Ts}, can be derived from the homogenous part of Eq. (6) as

$$\zeta_{\mathrm{Ts}} \equiv \frac{R}{2}\sqrt{\frac{C_{\mathrm{t}}}{L}}, \tag{11}$$

where index Ts denotes a serially connected TMD. We can then determine the requirements needed to create a resonance phenomenon in the serial circuit, i.e., the condition

$$0 \le \zeta_{\mathrm{Ts}} < 1. \tag{12}$$

First, we consider resistance *R*. Note that the resistor shown in Fig. 5 is not an electric load and that the actual electric load is between terminals *a* and *b*; instead, the inductor and the resistor in the figure are elements of a power supply. A larger electrical resistance load will result in increased damping and power consumption, and in a power supply, it is not desirable for energy to be consumed internally. Therefore, null resistance, i.e., $R = 0$, corresponds to the optimal situation, and no resistor should be connected within the serial power supply. In this case, the damping value in Eq. (11) becomes 0. Because this condition is satisfied in Eq. (12), a circuit with $R = 0$ can be used as a TMD vibration-powered generator.

Next, we consider the inductance value *L*. When $R = 0$, as determined above, the electrical angular frequency ω_{e} is given by

$$\omega_{\mathrm{e}} \equiv \frac{1}{\sqrt{L C_{\mathrm{t}}}}. \tag{13}$$

As the piezoelectric transducer attached to the host structure is used as a vibration-powered generator, the electrical frequency will match the structural vibration frequency ω_{s} (i.e., $\omega_{\mathrm{e}} = \omega_{\mathrm{s}}$). Inductance *L* then can be set to

$$L = \frac{1}{\omega_{\mathrm{s}}^2 C_{\mathrm{t}}}. \tag{14}$$

Finally, an equivalent circuit to the serial TMD connection shown in Fig. 5 is considered. Using Thevenin's theorem, we obtain

$$\left|V_{\mathrm{Ts}}\right| = \left|V_x\right|, \tag{15}$$

$$Z_{\mathrm{Ts}} = \sqrt{\left(\omega_{\mathrm{s}} L - \frac{1}{\omega_{\mathrm{s}} C_{\mathrm{t}}}\right)}, \tag{16}$$

$$\left|I_{\mathrm{Ts}}\right| \equiv \left|\frac{V_{\mathrm{Ts}}}{Z_{\mathrm{Ts}}}\right| = \frac{V_{x\mathrm{m}}}{\sqrt{\left(\omega_{\mathrm{s}} L - \frac{1}{\omega_{\mathrm{s}} C_{\mathrm{t}}}\right)}}. \tag{17}$$

Based on Eq. (14), Eqs. (15)-(17) can be transformed into

$$\left|V_{\mathrm{Ts}}\right| = \left|V_x\right|, \tag{18}$$

$$Z_{\mathrm{Ts}} \to 0, \tag{19}$$

$$\left|I_{\mathrm{Ts}}\right| \to \infty, \tag{20}$$

respectively. Noting the unchanged voltage, the decrease in internal impedance, and the increase in current, we see that the serial TMD generator possesses a current amplifying mechanism.

2.5 Parallel TMD generator

Fig. 6 shows an example of a parallel TMD connection in which the LCR damping ratio is given by

$$\zeta_{\mathrm{Tp}} \equiv \frac{1}{2R}\sqrt{\frac{L}{C_{\mathrm{t}}}}. \tag{21}$$

Here, index Tp denotes a parallel-connected TMD. As in the serial case above, the resonance condition for this circuit is expressed as

$$0 \le \zeta_{\mathrm{Tp}} < 1. \tag{22}$$

To minimize power consumption within the supply, it is preferable to use an infinitely large resistance (i.e., $R = \infty$), and, as such, it is best not to connect a resistor in parallel. The conclusion that no resistor should be connected in the parallel TMD generator is the same as that for a serial connection. Additionally, the resonance vibration frequency and impedance L are also the same as in the serial TMD. Applying Thevenin's theorem to the parallel TMD circuit produces

$$\left|V_{\mathrm{Tp}}\right| = \frac{\omega_{\mathrm{s}} L}{\sqrt{\left(\omega_{\mathrm{s}} L - \frac{1}{\omega_{\mathrm{s}} C_{\mathrm{t}}}\right)^2}}\left|V_x\right|, \tag{23}$$

$$Z_{\mathrm{Tp}} = \frac{1}{\sqrt{\left(\omega_{\mathrm{s}} L - \frac{1}{\omega_{\mathrm{s}} C_{\mathrm{t}}}\right)^2}}\frac{L}{C_{\mathrm{t}}}, \tag{24}$$

$$\left|I_{\mathrm{Tp}}\right| \equiv \left|\frac{V_{\mathrm{Tp}}}{Z_{\mathrm{Tp}}}\right| = \omega_{\mathrm{s}} C_{\mathrm{t}} V_{x\mathrm{m}}. \tag{25}$$

Substitution of Eq. (14) into Eqs. (23)-(25) results in the transformed equations

$$\left|V_{\mathrm{Tp}}\right| \to \infty, \tag{26}$$

$$Z_{\mathrm{Tp}} \to \infty, \tag{27}$$

$$\left|I_{\mathrm{Tp}}\right| = \omega_{\mathrm{s}} C_{\mathrm{t}} V_{x}, \tag{28}$$

respectively. From the increase in both voltage and internal impedance and the unchanged current, it is apparent that the parallel TMD generator has a voltage amplifying mechanism.

3. TMD vibration-powered generation experiment

3.1 Experimental equipment for vibrational power generation

An overview of the experimental equipment used in the vibrational power case is shown in Fig. 7. The vibrating structure consists of a 300 × 270 × 1.0 mm carbon fiber reinforced plastic (CFRP) plate (see Fig. 8) that is clamped on the bottom and has a layer configuration of $[90/45/\text{-}45/0]_2$ (the material characteristics of the CFRP plate are detailed in Table 1). A 30×30×0.25 mm piezoelectric transducer (S-SY1C6H, Fuji Ceramic Corp.) is used for power generation (the white square in Fig. 8) and is attached to the location shown in Fig. 7. A piece of piezoelectric material (S-SY1C6H, Fuji Ceramic Corp.) with the same dimensions is used to excite structural vibration and is attached on the other side of the plate. The piezoelectric patches, which are all composed of ceramic-type materials, are each covered by two thin metal electrodes on the top and bottom surfaces and have a polarization direction running from bottom to top. Their surface areas are quite large considering their thicknesses.

The first vibrational mode of this system has a natural frequency of 14.0 Hz. Deformation at the corner of the CFRP plate (shown by the spot in Fig. 7) is measured using a laser displacement meter (LK-030/LK-2000, KEYENCE Corp.). In all of the following experiments, the CFRP plate was excited to vibrate in such a way that its amplitude of vibration at the corner was exactly 1 mm. As the laser displacement meter was used only to maintain vibration test conditions, the electrical power consumed by the displacement meter did not need to be taken into consideration. Serially and parallel-connected TMD generators were connected to a diode bridge in a similar manner as shown in the circuit in Fig. 2, and based on Eq. (14), the inductances were set to L = 1.16 kH. Owing to this large value of inductance, a simulated inductor was used in the experiments. We employed the voltage follower circuit (Cerni and Foster 1962) composed of an operational amplifier to avoid unnecessary consumption during the measurement of generated power. The voltage follower provided very high input impedance to the electric components while isolating them from the measurement circuits, allowing small amounts of power to be measured with great accuracy.

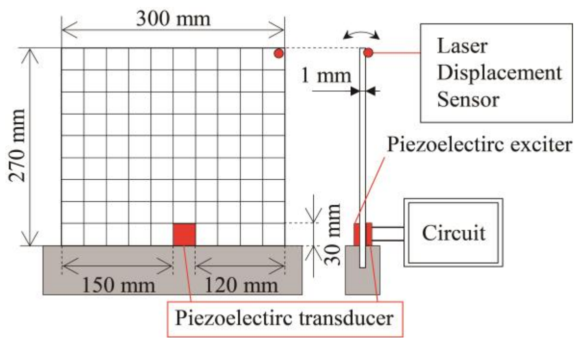

Fig. 7 Experimental equipment used in vibration-powered generation

Fig. 8 Photograph of CFRP plate clamped on bottom and piezoelectric transducer (white square)

3.2 Measurement of power generation with a resistive load

We then measured the power generated by the TMD generator with a resistive load, i.e., using a resistor as an electric load. Fig. 9 shows the measurement results for power harvested at the load resistor in this case. The dots in the figure represent measurement points, and a fitting curve is drawn to make the trend easier to understand. Comparing the maximum levels of generated power, it can be seen that the IM generator produces 13 μW at a load resistance of 200 kΩ, the serial TMD generator produces 31 μW at a load resistance of 100 kΩ, and a parallel TMD generator produces 28 μW at a load resistance of 500 kΩ. It is immediately apparent that both the serial and parallel TMD generators outperform the conventional IM generator over all ranges of resistance, with the serial and parallel generators producing 238 and 215% more power, respectively, than the conventional IM generator. Additionally, the optimal resistance of the serial generator is lower than the others; this confirms Eqs. (19) and (27), in which the internal impedance of a serial generator is lower than that of a parallel generator.

Table 1 Material properties of CFRP plat

	E_{11}[GPa]	E_{22}[GPa]	G_{12}[GPa]	ν_{12}	ρ [kg/m^3]
	127.0	11.0	6.3	0.3	1540

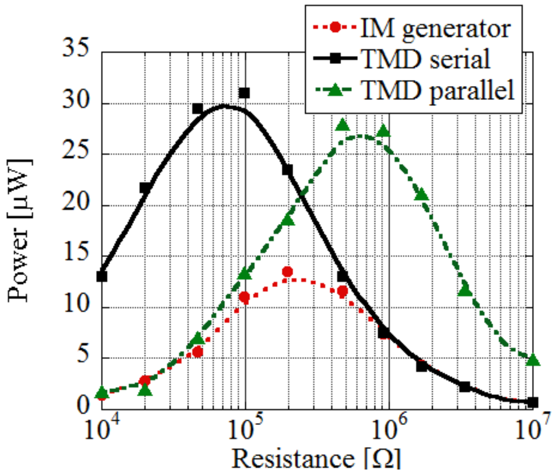

Fig. 9 Comparison of power output of three generators

In practical terms, actual circuits will have resistance components and it is difficult to completely tune TMD resistance and frequency parameters; thus, the internal resistance is never likely to be $0\,\Omega$ as indicated in Eq. (19), nor is it likely to be $\infty\,\Omega$ as indicated in Eq. (27). Nevertheless, in view of the experimental results above, a theoretical development using the equations given here is useful in expressing qualitative trends in internal impedance for each type of TMD connectivity.

3.3 Measurement of energy generation of a storage capacitor

The stored energy in a storage capacitor can be experimentally measured by connecting the capacitor to the TMD generator. Figure 10 shows the stored voltage of a serial TMD generator at several storage capacitances. We can see that the charging time of the serial generator is short up to a voltage of 2.7 V, but from there to 3.6 V it increases; i.e., after 2.7 V the voltage stored in the serial TMD generator increases gradually until it becomes saturated at 3.6 V.

Fig. 11 shows the stored voltage of a parallel TMD generator at several storage capacitances. In this case, the voltage increases as a linear function of capacitance, and the voltage stored in the parallel TMD generator is much higher than that stored in the serial generator, which is in agreement with our previous conclusion that the parallel TMD generator possesses a voltage amplifying mechanism (Section 2.5).

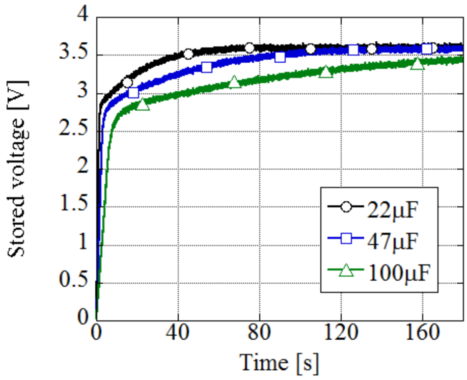

Fig. 10 Voltage stored in serial TMD generator

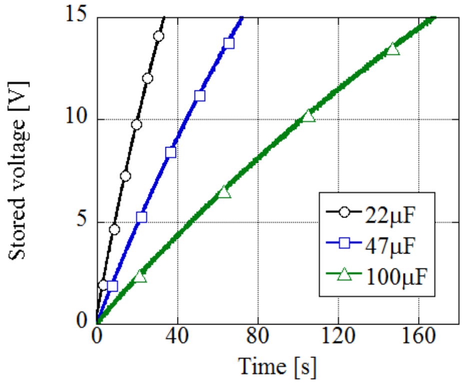

Fig. 11 Voltage storedin parallel TMD generator

Fig. 12 shows a comparison of stored energy among the three types of generator (IM, serial TMD, and parallel TMD) at storage capacitance $C_S = 47\ \mu\text{F}$. At t = 60 s, the energies stored in the IM, serial, and parallel generators are 0.3, 0.26, and 5.0 mJ, respectively. Clearly, the amount of energy stored in the parallel TMD generator is by far the largest and represents a 16-fold increase over the conventional IM generator.

Fig. 13 shows a comprehensive comparison of charging times for the three generator types. The serial TMD generator has the shortest charging time of the three, while the parallel generator has a shorter charging time than the conventional IM generator, which represents a preferable result for both types of proposed TMD generator. From this, it can be seen the optimal type of TMD generator depends on the application; the parallel generator should be used when stored energy is important (Fig. 12), while the serial generator should be used when the charging time is important (Fig. 13). We should select which of the serial or parallel TMD generator, depending on the application purpose of power generation.

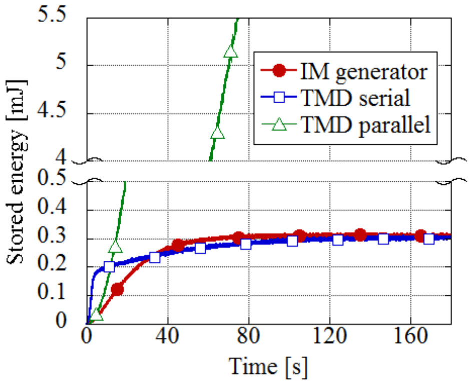

Fig. 12 Stored energy comparison

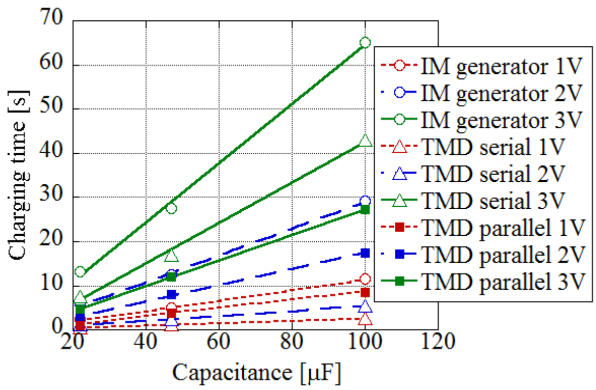

Fig. 13 Charging time for each vibration-powered generator type

4. Wireless monitoring using vibration-powered TMD generator

4.1 Overall wireless monitoring configuration

The vibration-powered TMD generator described in the previous section can be used as the driving power supplier of a wireless monitoring system utilized for structural health monitoring. Figure14 shows a schematic of the wireless monitoring system fabricated for this study. The overall system can be divided into a power source and a wireless sensor system; the power source has the same configuration as the vibration-powered generator described previously. The wireless sensor system consists of a sensor, a wireless transmitter (TY24FM-e2024, NEC Corp.), and a PIC (PIC16F88, MICROCHIP Inc.) that processes sensor signals and controls the wireless transmitter. Because piezoelectric sensors do not require a power supply, a piezoelectric transducer (S-SY1C6H, Fuji Ceramic Corp.) was used as a vibration sensor for this study. All of the power needed to activate the PIC and the wireless transmitter was supplied by the generator.

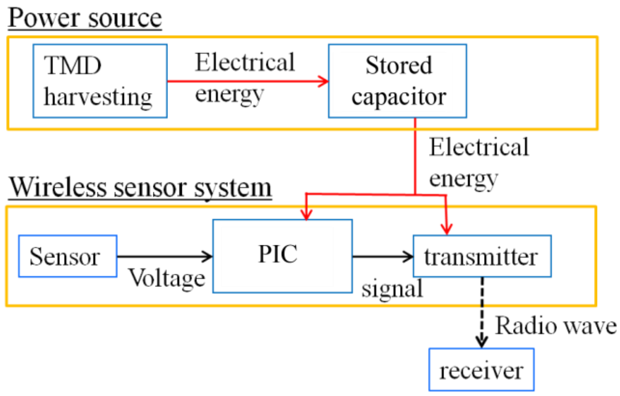

Fig. 14 Comprehensive schematic view of wireless SHM system using TMD

4.2 Wireless monitoring unit

Fig. 15 shows the configuration of the wireless transmitter. A storage capacitor is connected to the PIC and the wireless transmitter, and wireless transmission is controlled by the PIC. The processing order is as follows. First, voltage from the sensor is input to the analog input port (AN0-17). Second, the analog signal is converted into a one-byte digital signal by the analog-digital (AD) conversion module built into the PIC. Third, the converted 13-byte signal is sent to the wireless transmitter. A universal synchronous asynchronous receiver transmitter (USART) that sets the asynchronous serial transmission format is used for communication between the PIC and the wireless transmitter; finally, the wireless transmitter radiates the data.

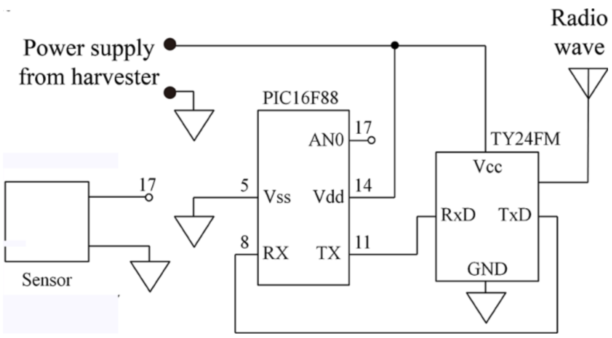

Fig. 15 Wireless transmitter configuration for SHM

Importantly, the wireless monitoring unit is designed to radiate sensor data in intervals rather than continuously; this is because structures usually deteriorate gradually, so intermittent communication is sufficient in order to grasp an accurate data of structural health. For this purpose, some energy is stored in the storage capacitor and then dissipated over short time intervals in radiating the data.

4.3 Interpolation analysis of charging time

The PIC and transmitter can be activated only when the stored voltage is within the operational voltage range of these components; thus, the stored voltage range must be from 2to 3V. The consumed energy in wireless transmission U is expressed as

$$U = \frac{1}{2} C_{\mathrm{s}} \left(V_{\mathrm{a}}^{2} - V_{\mathrm{b}}^{2} \right), \tag{29}$$

where V_{b} is the voltage stored before the transmitter is driven and V_{a} is the stored voltage remaining after driving. The energy consumed in activating the transmitter is 99 mW. Based on the value of storage capacitance determined in Eq. (29), a 39.6 mF capacitor is used.

We can then compare the charging time to storage capacitance needed for the three types of vibration-powered generators (IM, serial TMD, and parallel TMD). To calculate the charging time for the IM generator, $T_{\mathrm{IM}}(\text{stored voltage})$ can be expressed in units of seconds as a function of the storage capacitance C_{s}, which is in units of microfarads. From Fig. 13, interpolating equations of the charging time can be linearized as

$$T_{\mathrm{IM}}(3\mathrm{V}) = 0.670\, C_{\mathrm{s}} - 2.47, \tag{30}$$

$$T_{\mathrm{IM}}(2\mathrm{V}) = 0.300\, C_{\mathrm{s}} - 1.11. \tag{31}$$

The charging time needed for the stored voltage to rise from 2 to 3 V can then be calculated using $T_{\mathrm{IM}}(3\mathrm{V}) - T_{\mathrm{IM}}(2\mathrm{V})$. For a 39.6 mF storage capacitor, the charging time needed to attain wireless monitoring capacity is therefore 244 min. Similarly, Fig. 13 gives the charging time of the serial TMD generator as

$$T_{\mathrm{Ts}}(3\mathrm{V}) = 0.4 C6_{\mathrm{s}} - 0 \tag{32}$$

$$T_{\mathrm{Ts}}(2\mathrm{V}) = 0.0553\, C_{\mathrm{s}} - 0.168. \tag{33}$$

Using a 39.6 mF storage capacitor again, the charging time needed for wireless monitoring is 267 min for the serial generator. Again from Fig. 13, we find that the charging time of the parallel TMD generator is given by

$$T_{\mathrm{Tp}}(3\mathrm{V}) = 0.287\, C_{\mathrm{s}} - 1.51, \tag{34}$$

$$T_{\mathrm{Tp}}(2\mathrm{V}) = 0.185\, C_{\mathrm{s}} - 0.964. \tag{35}$$

This results in a charging time to wireless monitoring of 67 min for a parallel generator with a storage capacitance of 39.6 mF. As these charging times are simply predictions from Eqs. (30)-(35)

using limited charging data, they are compared to the actual measurement results in the next section.

4.4 Integration of TMD generator and wireless monitoring

We then experimentally measured the actual charging times for each generator type with a storage capacitance of 39.6 mF, and the results of this are compared with the predictions from linear formulation in Section 4.3 in Table 2. From the table, it can be seen that the predictions are in close agreement with the experimental measurements, which indicates that the charging time is in fact proportional to capacitance over a wide range of conditions.

Fig. 16 shows the results of wireless monitoring experiments using the proposed self-reliant system with a parallel TMD generator. This figure shows both the sensor and the received voltages, and each sensor signal was transmitted wirelessly in intervals (i.e., every 67 min). As the sensor and received voltage figures closely agree, it seems likely that such a self-reliant SHM system can be practically developed and used. As the system tested in the wireless monitoring experiment is intended for structural health monitoring, the power from the TMD generator was used to activate the wireless transmitter. These results confirmed that the TMD generator can be successfully used as a driving power supplier for a self-reliant SHM system usable. Our proposed self-reliant SHM system is promising for the usage of various applications and at a variety of sites, for instance, isolated structures, moving vehicles, long bridges, elevated expressways, or rotating devices such as turbine blades or automobile tires.

In this paper, the experimental results were produced using a 300×270×1.0 mm CFRP plate and a single, very small piezoelectric transducer. Although this represents a laboratory scale (i.e., small) vibrational unit, both the charging time and the generated power can be dramatically improved in implementing large-scale host structures and multiple piezoelectric transducers. This paper focused on proving the concept of a vibration-powered generator for a self-reliant SHM; in the next report, more sophisticated SHM applications will be presented.

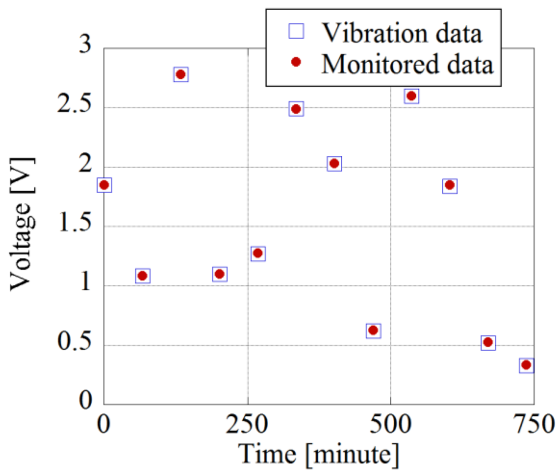

Fig. 16 Wireless monitoring experiment with parallel TMD generator

Table 2 Charging time for each type of vibration-powered generation

	IM	TMD serial	TMD parallel
Analysis prediction	244 min	267 min	67 min
Actual measurement	249 min	273 min	67 min

5. Conclusions

In this study, an electrically self-reliant SHM system using a proposed vibration-powered generation system based on a TMD mechanism was proposed and experimentally verified. It was shown that the SHM wireless transmitter could be activated and communication could be conducted using only electrical power from a TMD vibration-powered generator. The charging time of the TMD generator is also shorter than that of a conventional IM generator based on the impedance matching method, and the amount of harvested electrical energy is increased 16-fold. We clarified that either a serial or parallel configuration for TMD generation can be selected for use depending on whether energy storage or charging time is more important. The TMD generator can be successfully used as an activating power supplier for electrically self-reliant SHM systems. A wide range of vibration-powered generation data was obtained and formulated as interpolation equations by varying the storage capacitance. Finally, we validated the applicability of self-reliant SHM systems in a wireless monitoring experiment.

References

Badel, A., Guyomar, D., Lefeuvre, E. and Richard, C. (2006), "Piezoelectric energy harvesting using a synchronized switch technique", *J. Intel. Mat. Syst. Str.*, **17**(9), 831-839.

Beeby, S. and White, N. (2010), *Energy-Harvesting for Autonomous Systems (Smart Materials, Structures, and Systems)*, ArtechHouse.

Carden, E.P. and Fanning, P. (2004), "Vibration based condition monitoring: a review", *Struct. Health Monit.*, **3**(4), 355-377.

Cerni, R.H. and Foster, L.E. (1962), *Instrumentation for Engineering Measurement*, Wiley, New York.

Cho, S., Jo, H., Jang, S., Park, J., Jung, H.J., Yun, C.B., Spencer, Jr. B.F. and Seo, J.W. (2010), "Structural health monitoring of a cable-stayed bridge using wireless smart sensor technology: data analyses", *Smart Struct. Syst.*, **6**(5), 461-480.

Chong, S.Y., Lee, J.R. and Shin, H.J. (2010), "A review of health and operation monitoring technologies for trains", *Smart Struct. Syst.*, **6**(9), 1079-1105.

Cornwell, P.J., Goethal, J., Kowko, J. and Daminakis, M. (2005), "Enhancing energy harvesting using a tuned auxiliary structure", *J. Intel. Mat. Syst. Str.*, **16**, 825-834.

Den Hartog, J.P. (1984), *Mechanical Vibrations*, Dover, New York.

Fan, W. and Qiao, P. (2011), "Vibration-based damage identification methods: a review and comparative study", *Struct. Health Monit.*, **10**(1), 83-111.

Guyomar, D., Badel, A., Lefeuvre, E. and Richard, C. (2005), "Toward energy harvesting using active materials and conversion improvement by nonlinear processing", *IEEE T. Ultrason. Ferr.*, **52**, 584-595.

Hagood, N.W. and von Flotow, A. (1991), "Damping of structural vibrations with piezoelectric materials and passive electrical networks", *J. Sound Vib.*, **146**(2), 243-268.

Hollkamp, J.J. (1994), "Multimodal passive vibration suppression with piezoelectric materials and resonant shunts", *J. Intel. Mat. Syst. Str.*, **5**(1), 49-57.

Hu, N., Cai, Y., Zhu, G., Tsuji, C., Liu, Y., Alamusi and Cao, Y. (2012), "Characterization of damage size in metallic plates using Lamb waves", *Struct. Health Monit.*, **11**(2), 125-137.

Kazmierski, T.J. and Beeby, S. (2010), *Energy Harvesting Systems: Principles, Modeling and Applications*, Springer.

Kim, S., Clark, W.W. and Wang, Q. (2005), "Piezoelectric energy harvesting with a clamped circular plate: analysis", *J. Intel. Mat. Syst. Str.*, **16**, 847-854.

Kong, N., Ha, S.D., Erturk, A. and Inman, D.J. (2010), "Resistive impedance matching circuit for piezoelectric energy harvesting", *J. Intel. Mat. Syst. Str.*, **21**, 1293-1305.

Kozlowski, M.V., Cole, D.G. and Clark, R.L. (2011), "A comprehensive study of the RL series resonant shunted piezoelectric: a feedback controls perspective", *J. Vib. Acoust*., **133**, Article No. 011012-1.

Lefeuvre, E., Audigier, D., Richard, C. and Guyomar, D. (2007), "Buck-boost converter for sensorless power optimization of piezoelectric energy harvester", *IEEE T. Power Electr.*, **22**, 2018-2025.

Lesieutre, G.A., Ottman, G.K. and Hofmann, H.F. (2003), "Damping as a result of piezoelectric energy harvesting", *J. Sound Vib*., **269**(3-5), 991-1002.

Li, P., Gu, H., Song, G., Zheng, R. and Mo, Y.L. (2010), "Concrete structural health monitoring using piezoceramic-based wireless sensor networks", *Smart Struct. Syst.*, **6**(5), 731-748.

Lynch, J.P. (2005), "Design of a wireless active sensing unit for localized structural health monitoring", *J. Struct. Control Health Monit.*, **12**(3-4), 405-423.

Makihara, K., Onoda, J. and Miyakawa, T. (2006), "Low energy dissipation electric circuit for energy harvesting", *Smart Mater. Struct*., **15**(5), 1493-1498.

Makihara, K., Onoda, J. and Minesugi, K. (2007), "Using tuned electrical resonance to enhance bang-bang vibration control", *AIAA J*., **45**(2), 497-504.

Makihara, K., Takeuchi, S., Shimose, S. and Onoda, J. (2012), "Innovative digital self-powered autonomous system for multimodal vibration suppression", *AIAA J*., **50**(9), 2004-2011.

Morgan, R.A. and Wang, K.W. (2002), "Active-passive piezoelectric absorber for systems under multiple non-stationary harmonic excitation", *J. Sound Vib*., **255**(4), 685-700.

Ottman, G.K., Hofmann, H.K., Bhatt, A.C. and Lesieutre, G.A. (2003), "Optimized piezoelectric energy harvesting circuit using step down converter in discontinuous conduction mode", *IEEE T. Power Electr.*, **18**(2), 696-703.

Qiu, J., Jiang, H., Hongli, J. and Kongjun, Z. (2009), "Comparison between four piezoelectric energy harvesting circuits", *Front. Mech. Eng. China*, **4**, 153-159.

Shen, H., Qiu, J., Ji, H., Zhu, K. and Balsi, M. (2010), "Enhanced synchronized switch harvesting: a new energy harvesting scheme for efficient energy extraction", *Smart Mater. Struct*., **19**, Article No. 115017.

Wang, Y. and Inman, D.J. (2011), "Comparison of control laws for vibration suppression based on energy consumption", *J. Intel. Mat. Syst. Str.*, **22**(8), 795-809.

Wu, S. (1996), "Piezoelectric shunts with a parallel R-L circuit for structural damping and vibration control", *Proc. SPIE Smart Mater. Struct. Conf.*, SPIE Vol. 2720, Soc. Photo-Optical Inst. Eng., Bellingham, WA.

Wu, W.J., Wickenheiser, A.M., Reissman, T. and Garcia, E. (2009), "Modeling and experimental verification of synchronized discharging techniques for boosting power harvesting from piezoelectric transducers", *Smart Mater. Struct*., **18**(5), Article No. 055012.

CC